

HiPrune: Training-Free Visual Token Pruning via Hierarchical Attention in Vision-Language Models

Jizhihui Liu, Feiyi Du^{*}, Guangdao Zhu^{*}, Niu Lian, Jun Li, Bin Chen[†]

Harbin Institute of Technology, Shenzhen
2023112090@stu.hit.edu.cn, chenbin2021@hit.edu.cn

Abstract

Vision-Language Models (VLMs) encode images into lengthy sequences of visual tokens, leading to excessive computational overhead and limited inference efficiency. While prior efforts prune or merge tokens to address this issue, they often rely on special tokens (e.g., CLS) or require task-specific training, hindering scalability across architectures. In this paper, we propose **HiPrune**, a training-free and model-agnostic token **Pruning** framework that exploits the **Hierarchical** attention structure within vision encoders. We identify that middle layers attend to object-centric regions, while deep layers capture global contextual features. Based on this observation, HiPrune selects three types of informative tokens: (1) Anchor tokens with high attention in object-centric layers, (2) Buffer tokens adjacent to anchors for spatial continuity, and (3) Register tokens with strong attention in deep layers for global summarization. Our method requires no retraining and integrates seamlessly with any ViT-based VLM. Extensive experiments on LLaVA-1.5, LLaVA-NeXT, and Qwen2.5-VL demonstrate that HiPrune achieves state-of-the-art pruning performance, preserving up to **99.3%** task accuracy with only **33.3%** tokens, and maintaining **99.5%** accuracy with just **11.1%** tokens. Meanwhile, it reduces inference FLOPs and latency by up to **9×**, showcasing strong generalization across models and tasks. Code is available at <https://github.com/Danielement321/HiPrune>.

Introduction

Built on the success of Large Language Models (LLMs) (Touvron et al. 2023; Yang et al. 2025a), Vision Large Models (VLMs) have shown great capacity in image understanding (Team et al. 2023; Hurst et al. 2024; Liang et al. 2024), visual reasoning (Hong et al. 2025), and even downstream tasks like robot manipulation (Kim et al. 2024; Cen et al. 2025). VLMs commonly comprise a vision encoder (Radford et al. 2021; Zhai et al. 2023), an adaptor, and an LLM. The vision encoder is a vision transformer (ViT) (Dosovitskiy et al. 2021; Vaswani et al. 2017) that encodes the image into a sequence of tokens. Despite similarity in structure, VLMs are usually slower than similarly sized LLMs and more memory-hungry, constraining their usability in real deployment. One of the main causes is the overly long visual

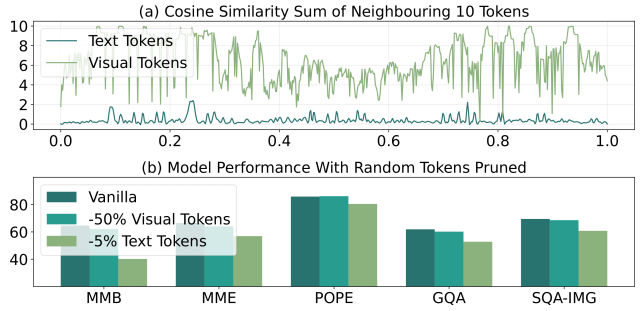


Figure 1: **Redundancy analyses on visual tokens.** (a) The sum of cosine similarity between each token and neighbouring 10 tokens. (b) The performance of LLaVA-1.5-7B when randomly removing 50% visual tokens or 5% text tokens.

token sequences, which account for the biggest proportion of inputs. In LLaVA-1.5 (Liu et al. 2023, 2024a), an image is encoded into 576 tokens, much longer than its textual counterparts (Zhang et al. 2025a). For VLMs that incorporate a native dynamic-resolution encoder (Bai et al. 2025), one high-resolution webpage snapshot may require more than 10,000 tokens, resulting in a substantial computational cost and GPU memory allocation.

Although visual tokens constitute the majority of VLM input sequences, their necessity remains questionable. Empirically, humans can still recognize image content even under low resolution, blur, or partial occlusion. Similarly, Masked Autoencoders (MAE) (He et al. 2022) demonstrate that models retain learning ability even when over 75% of visual tokens are masked, suggesting many tokens are not essential. To further validate this, we conduct two pilot studies. In Fig. 1(a), we compare the cosine similarity between each token and its 10 neighbors for both visual and textual tokens. Visual tokens exhibit significantly higher redundancy, with many reaching near-maximal similarity scores. In Fig. 1(b), we assess the impact of random token removal: pruning 50% of visual tokens causes a smaller performance drop than removing merely 5% of textual tokens, while yielding substantial reductions in FLOPs. Moreover, prior work (Chen et al. 2024a; Zhang et al. 2025d) observes that visual tokens receive markedly less attention from the LLM decoder compared to text tokens. Collectively, these findings point

^{*}These authors contributed equally.

[†]Corresponding author.

to a key insight: **visual tokens are highly redundant**, and pruning them offers an effective path toward improving efficiency without significantly sacrificing performance.

Many approaches seek to reduce the number of visual tokens to overcome the computational burden. Several approaches (Hu et al. 2024; Zhang et al. 2025d) adopt a Q-Former (Li et al. 2023a) to fuse the abundant image tokens into fewer learned query tokens, however, necessitating extra training and causing potential damage to VLM’s already-learned representation. Some methods (Bolya et al. 2023a; Alvar et al. 2025) draw inspiration from the similarity or diversity of tokens and adopt merging or pruning to accelerate VLM. These methods compress image information into fewer tokens but lack explainability and tend to overlook crucial details. In transformer (Vaswani et al. 2017), the attention score controls the information flow from layer to layer, and thus can be seen as an indicator of the importance of the current token (Vaswani et al. 2017). Based on this theory, many approaches (Zhang et al. 2025b; Arif et al. 2025; Yang et al. 2025b) prune tokens according to their attention score with the `CLS` token. However, not every vision encoder features such a token (e.g., SigLIP (Zhai et al. 2023)), constraining these methods’ adaptation for universal VLMs (Bai et al. 2025; Chen et al. 2024b).

In contrast to prior attention-based approaches that rely on text-image cross-attention from the LLM decoder to prune visual tokens (Chen et al. 2024a; Xing et al. 2025), we shift the focus to the vision encoder and exploit its intrinsic hierarchical attention structure. Through comprehensive qualitative and quantitative analysis across layers, we reveal that vision encoders process visual information in a progressive and structured hierarchy, where different layers attend to distinct semantic levels. Specifically, middle layers predominantly capture object-centric features, while deeper layers encode global contextual representations. Importantly, this hierarchical pattern is consistently observed across a variety of vision encoders (Radford et al. 2021; Zhai et al. 2023; Touvron et al. 2021), regardless of architecture design or pre-training data, even including world model encoders (Assran et al. 2025), suggesting that such attention stratification is model-agnostic and universally present.

Building on this observation, we introduce **HiPrune**, a *training-free* and *model-agnostic* visual token pruning method for VLM inference acceleration. The core idea is to preserve a compact subset of tokens that collectively retain both fine-grained and global visual information, guided by the **hierarchical attention** within the vision encoder. Specifically, we first extract attention maps from a designated *object layer* l , selecting tokens with the highest attention scores as **Anchor Tokens**, which primarily correspond to object-centric regions. To enhance spatial continuity and suppress potential noise in attention estimation, we augment these anchors with adjacent **Buffer Tokens**. Together, anchor and buffer tokens encode detailed local semantics. The remaining token budget is allocated to **Register Tokens**, selected from the *output layer* based on attention scores. As shown in prior work (Dariset et al. 2024; Arif et al. 2025) and further validated in our study, these register tokens capture **global contextual features**, enabling a holistic repre-

sentation of the image under tight token constraints. Combining the three types of tokens, HiPrune preserves most of the original model’s performance while requiring much less computation and memory. When applied to LLaVA-1.5, HiPrune maintains **99.3%** of original performance while requiring only **33.3%** tokens. On LLaVA-NeXT, HiPrune even slightly boosts the overall performance by **2.6%** with **22.2%** tokens, alongside bringing a **6 \times** FLOPs reduction. With a different encoder and dynamic token length setting, HiPrune achieves state-of-the-art (SOTA) on Qwen (Bai et al. 2025), confirming its versatility.

Our main contributions are summarized as follows:

- We conduct a comprehensive analysis of the hierarchical attention patterns in vision encoders, revealing that *middle layers focus on object-centric details while deep layers attend to global contextual information*. This pattern is shown to be universal, showing little correlation with model architectures or pre-training data.
- We propose HiPrune, a *training-free* and *model-agnostic* visual token pruning framework that leverages hierarchical attention to select informative tokens, enabling efficient inference without altering original VLM structure.
- Extensive experiments on LLaVA-1.5, LLaVA-NeXT, and Qwen2.5-VL demonstrate that HiPrune achieves SOTA accuracy-efficiency trade-offs, preserving up to **99.3%** performance with only **33.3%** tokens and reducing inference FLOPs by up to **9 \times** .

Related Works

Vision-Language Models

VLMs (Bai et al. 2023; Li et al. 2023a; Hurst et al. 2024; Team et al. 2023; Chen et al. 2024b) have achieved impressive performance in various multimodal tasks. These models are typically composed of an image encoder, a text encoder, and an LLM. In the input sequence fed to the LLM, visual tokens often constitute a significant portion. For example, an input image is encoded into 576 tokens in LLaVA-1.5 (Liu et al. 2023, 2024a). To improve the model’s capacity for fine-grained understanding, some models, such as LLaVA-NeXT (Liu et al. 2024b) and LLaVA-UHD (Guo et al. 2024), increase the resolution of the input image, which further raises the number of visual tokens in the sequence. The excessive number of visual tokens leads to considerable computational overhead and adversely affects the inference speed of the model, constraining its practical deployment. This motivates the need for visual token compression techniques that aim to reduce redundancy while preserving model performance.

Visual Token Compression Methods

Most visual token compression methods adopt a prune or merge strategy. FastV (Chen et al. 2024a) is a representative pruning method that compresses visual tokens by discarding those with low attention scores in the LLM. Following this work, PDrop (Xing et al. 2025) and TRIM (Song et al. 2025) propose to employ the text-image attention to prune tokens, which brings extra computation from text-image attention. FasterVLM (Zhang et al. 2025b), HiRED (Arif et al.

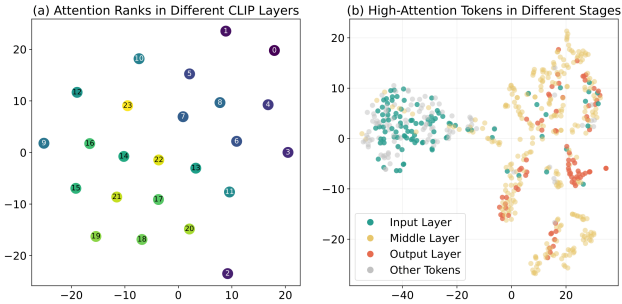


Figure 2: **Hierarchical attention pattern in CLIP.** (a) Attention rankings of different layers. Most layers are neighbouring their adjacent layers. (b) Top 50% attentive tokens from different CLIP layers. The attention shifts from one cluster to another, showing a gradual and continuous transition, bridged by the middle-layer attention. Please refer to the supplementary material for a detailed explanation.

Layer	CLIP-L	CLIP-B	SigLIP	SigLIP2	DeiT	VJEPAP2
1	0.58×	0.34×	0.57×	0.62×	0.27×	0.82×
L/2	1×	1×	1×	1×	1×	1×
L	0.80×	0.79×	0.66×	0.64×	0.59×	0.26×

Table 1: **IoU of object segmentation mask and top 10% high-attention tokens.** Higher values stand for more overlap on objects in the image. ‘L’ denotes the total layers in the encoder. The data is normalized for a better comparison.

2025), VisionZip (Yang et al. 2025b) solely rely on the attention in the vision encoder, mostly on the attention from CLS token, making them model-sensitive. Apart from the drop strategy, ToMe (Bolya et al. 2023b) employs a merge approach by reducing the number of visual tokens according to their similarity. Subsequently, many researchers have proposed their merging methods, such as LLaVA-MINI (Zhang et al. 2025d) and MQT-LLaVA (Hu et al. 2024). Most merging methods necessitate extra training or functions not as efficient as dropping methods, since the merging is usually gradual across multiple layers and not compatible with FlashAttention (Dao et al. 2022). In this work, we show that pruning tokens purely based on the vision encoder’s inherent hierarchical attention pattern can achieve outstanding results while avoiding special tokens and unnecessary complexity.

Motivated Insights

Hierarchical Representation Patterns in Vision Encoders

To better understand the information flow in VLMs, we investigate the internal structure of vision encoders and identify a progressive attention hierarchy:

- **Layer-wise continuity:** Visualizing attention rankings across layers with t-SNE (Maaten and Hinton 2008) (Fig. 2(a)) reveals a smooth, ordered trajectory, indicating representations evolve gradually through network.

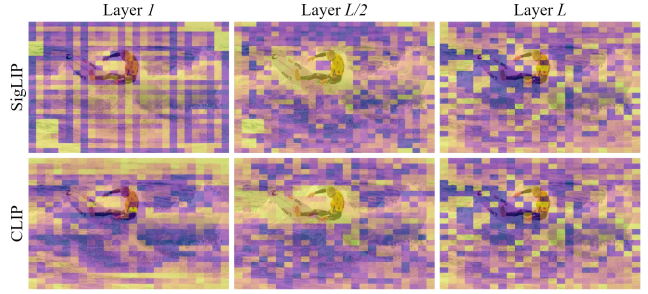


Figure 3: **Attention map for different layers of SigLIP and CLIP.** Patches with higher scores are in yellow. We can see that the middle layer is more object-centric.

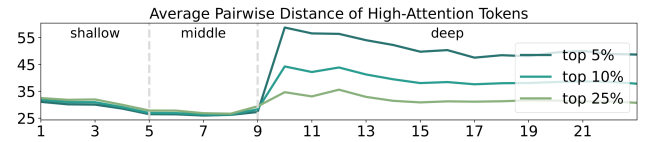


Figure 4: **Average pairwise distance of high-attention tokens from different layers in CLIP.** Based on the trend of dispersion, we divide CLIP into three phases.

- **Cluster transitions:** As shown in Fig. 2(b), high-attention tokens shift from one semantic cluster to another across layers, with middle layers bridging low-level input and high-level output representations.
- **Hierarchical abstraction:** This attention trajectory suggests an implicit encoding hierarchy—shallow layers retain noise, middle layers focus on semantic objects, and deep layers encode global context.

Semantic Focus of Middle and Deep Layers

By visualizing attention maps and correlating with ground-truth object regions, we identify distinct semantic roles of different encoder depths:

- **Object-centric middle layers:** Attention maps from middle layers (e.g., CLIP and SigLIP) align with salient objects in the image (the surf-man in Fig. 3).
- **Quantitative evidence:** IoU analyses on COCO (Lin et al. 2014) confirm that middle-layer attention overlaps more with object than shallow or deep layers (Table 1).
- **Global-context deep layers:** Deep-layer tokens exhibit uniform spatial distribution, serving as effective global summarizers even under constrained token budgets.

Guiding Layer Partition via Attention Dispersion

To inform token pruning design, we quantitatively analyze attention dispersion and define a principled layer partition:

- **Dispersion curve:** We compute the average pairwise distance among top-attention tokens per layer in CLIP (Fig. 4), revealing distinct phases.
- **Layer grouping:** Based on this, we categorize CLIP layers into three regions: shallow (1–4), middle (5–9), and

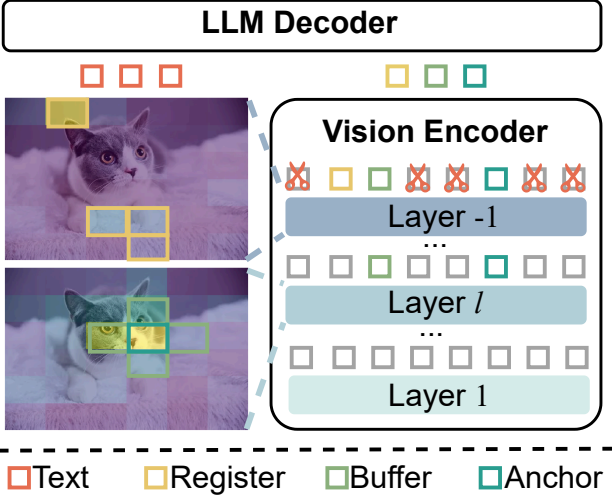


Figure 5: **An overview of HiPrune.** We first allocate anchor tokens that receive the highest attention in layer l and record buffer tokens around them. Then we allocate register tokens directly based on the last layer attention of the rest of the tokens. HiPrune only accesses the attention in the vision encoder while keeping the LLM unchanged.

deep (10+), capturing a transition from noise to object detail and finally to global information.

- **Architecture-agnostic validity:** This partition strategy generalizes across encoder architectures and supports the design of hierarchical pruning strategies like HiPrune.

Method

An overview of our method is depicted in Fig. 5. Given a token budget, we retain three kinds of tokens, i.e., anchor, buffer, and register tokens, according to hierarchical attention in the vision encoder and spatial relationship. In the following, we first revisit the self-attention, then we present the definition and preservation rationale for these tokens.

Preliminaries

In a ViT-based vision encoder, an image is first divided into multiple non-overlapping patches; after that, each patch is projected into a token $\mathbf{t} \in \mathbb{R}^d$. All the tokens form a token matrix $\mathbf{T} \in \mathbb{R}^{N \times d}$, where N denotes the number of patches in an image and d denotes the hidden dimension of the model. In each layer, the tokens are first multiplied by learnable $\mathbf{W}_Q, \mathbf{W}_K, \mathbf{W}_V \in \mathbb{R}^{d \times d}$ into $\mathbf{Q}, \mathbf{K}, \mathbf{V} \in \mathbb{R}^{N \times d}$, respectively. These three matrices are then divided into H heads with a shape of $\mathbf{Q}, \mathbf{K}, \mathbf{V} \in \mathbb{R}^{H \times N \times d_k}$, where $d_k = \frac{d}{H}$. The attention is computed by

$$\mathbf{A} = \text{softmax}\left(\frac{\mathbf{Q}\mathbf{K}^T}{\sqrt{d_k}}\right) \in \mathbb{R}^{H \times N \times N}. \quad (1)$$

The information sharing between tokens only takes place in Eq. 1. Intuitively, the more ‘important’ a token is, the more its value in every token’s new state, which is assigned

by \mathbf{A} . Therefore, in layer l , the importance of tokens can be weighted by their attention score:

$$\mathbf{a}^{[l]} = \frac{1}{H} \sum_{h=1}^H \sum_{n=1}^N \mathbf{A}^{[l]}[h, n, :], \quad (2)$$

$$= (a_1^{[l]}, a_2^{[l]}, \dots, a_N^{[l]}) \in \mathbb{R}^N. \quad (3)$$

Retained Tokens

Anchor tokens denote tokens with the highest attention score in the middle layers of the vision encoder. As discussed in our motivated insights, the middle layers tend to focus on the object features, manifested as higher attention scores for tokens related to the object. Based on this phenomenon, anchor tokens encode rich, detailed information about the raw image and should be retained when pruning.

Buffer tokens are tokens spatially adjacent to anchor tokens in the original image. As indicated by many studies (Darcel et al. 2024; Yang et al. 2024), noise exists in the attention map of ViTs. In Fig. 3, despite most high-attention tokens concentrating on the surf-man, a few tokens diffuse among the image, which may mislead the anchor tokens. To mitigate the noise issue and preserve the spatial relationship, we include tokens neighbouring the anchor as a buffer.

Register tokens receive top attention scores in the output layer of the vision encoder. In deep layers of the vision encoder, the high-attention tokens distribute uniformly across the image, serving as an ideal indicator of global information. To enhance the model’s overall understanding of an image, we supplement the token set with register tokens, which is a common practice in approaches for VLM token pruning (Zhang et al. 2025b; Arif et al. 2025; Zhang et al. 2025b).

Pruning Pipeline

Given a target token budget N' , we designate two key parameters, the object layer l and object proportion α , denoting the layer from which to determine anchor and buffer tokens, and the added-up proportion of them. Taking the cross strategy as an example (4 buffers around 1 anchor), we first draw the attention score $\mathbf{a}^{[l]}$ from the object layer l and calculate the number of anchor tokens by $N_a = \lceil \frac{\alpha * N'}{5} \rceil$. The anchor token indices set \mathcal{I}_A is decided by

$$\mathcal{I}_A = \{i \mid |\{j \mid a_j^{[l]} > a_i^{[l]}\}| < N_a\}. \quad (4)$$

Once the anchor tokens are decided, we proceed to retain buffer tokens. It is worth noting that the buffer selection scheme can be diverse, but little difference exists between choices as long as the size is big enough, which is to be discussed in our ablation studies. Assuming there are p patches in a row, buffer token indices \mathcal{I}_B is calculated by

$$\mathcal{I}_B = \cup \{\mathcal{I}_A - 1, \mathcal{I}_A + 1, \mathcal{I}_A - p, \mathcal{I}_A + p\} \cap [0, p^2 - 1]. \quad (5)$$

The register token selection occurs after anchor tokens and buffer tokens, given the attention score $\mathbf{a}^{[-1]}$ of the output layer of the vision encoder, the registers are selected by

$$\mathcal{I}_R = \{i \mid |\{j \mid a_j^{[-1]} > a_i^{[-1]}\}| < N' - |\mathcal{I}_A \cup \mathcal{I}_B| \quad (6)$$

$$\wedge i \notin \mathcal{I}_A \cup \mathcal{I}_B\}.$$

Method	Venue	GQA	MMB	MMB ^{CN}	MME	POPE	SQA ^{IMG}	VQA ^{V2}	VQA ^{Text}	VizWiz	Average
<i>Vanilla, 576 Tokens (100%)</i>											
LLaVA-1.5-7B	CVPR'24	61.9	64.7	58.1	1862	85.9	69.5	78.5	58.2	50.0	100.0%
<i>Retain 192 Tokens (33.3 %)</i>											
ToMe	ICLR'23	54.3	60.5	-	1563	72.4	65.2	68.0	52.1	-	88.5%
FastV	ECCV'24	52.7	61.2	57.0	1612	64.8	67.3	67.1	52.5	50.8	90.4%
HiRED [†]	AAAI'25	58.8	62.6	54.5	1742	83.0	67.9	75.0	-	51.1	96.4%
TRIM [†]	COLING'25	59.9	64.1	53.6	1765	87.1	67.8	76.2	54.9	50.4	97.1%
PyramidDrop	CVPR'25	57.3	63.3	56.8	1797	82.3	69.0	75.1	56.5	51.1	97.2%
VisionZip	CVPR'25	59.3	63.0	-	1783	85.3	68.9	76.8	57.3	-	97.7%
SparseVLM [†]	ICML'25	59.5	64.1	58.0	1780	85.4	68.8	77.0	57.7	50.6	98.6%
HiPrune	Ours	59.2	62.8	57.0	1814	86.1	68.9	76.7	57.6	54.5	99.3%
<i>Retain 128 Tokens (22.2%)</i>											
ToMe	ICLR'23	52.4	53.3	48.8	1343	62.8	59.6	63.0	49.1	50.2	83.0%
FastV	ECCV'24	49.6	56.1	56.4	1490	59.6	60.2	61.8	50.6	51.3	85.4%
HiRED [†]	AAAI'25	57.1	61.7	53.9	1714	79.8	68.1	73.5	-	51.4	95.0%
TRIM [†]	COLING'25	58.9	63.3	51.5	1732	87.2	68.4	74.8	52.7	50.6	95.7%
PyramidDrop	CVPR'25	57.1	61.6	56.6	1761	82.3	68.4	72.9	56.6	51.0	96.2%
VisionZip	CVPR'25	57.6	62.0	-	1762	83.2	68.9	75.6	56.8	-	96.2%
SparseVLM [†]	ICML'25	53.8	64.4	58.1	1761	85.0	68.5	76.3	56.7	50.2	97.0%
HiPrune	Ours	57.3	62.2	56.4	1782	82.8	68.3	74.9	56.64	54.3	97.5%
<i>Retain 64 Tokens (11.1%)</i>											
ToMe	ICLR'23	48.6	43.7	38.9	1138	52.5	50.0	57.1	45.3	50.2	73.1%
FastV	ECCV'24	46.1	48.0	52.7	1256	48.0	51.1	55.0	47.8	50.8	76.7%
HiRED [†]	AAAI'25	54.6	60.2	51.3	1595	73.7	68.2	69.8	-	53.3	91.8%
TRIM [†]	COLING'25	56.9	61.5	44.9	1603	86.7	69.0	71.9	50.0	50.6	92.1%
PyramidDrop	CVPR'25	47.5	58.8	50.5	1561	55.9	69.2	69.2	50.6	50.7	86.7%
VisionZip	CVPR'25	55.1	60.1	-	1690	77.0	69.0	72.4	55.5	-	92.7%
SparseVLM [†]	ICML'25	53.7	60.1	52.5	1559	77.5	69.7	70.2	53.4	50.4	91.8%
HiPrune	Ours	53.6	59.5	53.4	1646	73.0	68.9	69.2	54.9	54.4	92.7%

Table 2: **Results on LLaVA-1.5-7B.** All the methods are in a training-free way. ‘[†]’ denotes results reproduced by us.

It is notable that \mathcal{I}_A , \mathcal{I}_B , and \mathcal{I}_R are just the indices of tokens; the tokens for the LLM component are still chosen from the output layer of the vision encoder. After obtaining these token indices, HiPrune directly selects the corresponding tokens from the original token matrix $\mathbf{T} \in \mathbb{R}^{N \times d}$ and discards the rest, leaving a pruned token matrix

$$\mathbf{T}' = \mathbf{T}[\mathcal{I}_A \cup \mathcal{I}_B \cup \mathcal{I}_R, :] \in \mathbb{R}^{N' \times d}. \quad (8)$$

Experiments

Experiment Settings

Models. HiPrune is model-agnostic and training-free, applicable to any VLM with at least one vision encoder and an LLM. We conduct HiPrune on models with various vision encoders and visual token partition strategies. Following most previous work, we evaluate on LLaVA-1.5-7B (Liu et al. 2024a) and LLaVA-NeXT-7B (Liu et al. 2024b), which encode images into fixed-length token sequences. We also include evaluations on Qwen2.5-VL-3B-Instruct (Bai et al. 2025), which uses a dynamic-resolution ViT and encodes images into various-length sequences. All the models are

loaded with their officially released weights without further tuning except as specially mentioned.

Datasets. We conduct thorough experiments across various multimodal benchmarks, including visual question answering benchmarks such as GQA (Hudson and Manning 2019), SQA (Lu et al. 2022), VQAv2 (Goyal et al. 2017), MME (Fu et al. 2024), and TextVQA (Singh et al. 2019). Additionally, we include POPE (Li et al. 2023b) and VizWiz (Gurari et al. 2018) to study the hallucination when visual tokens are pruned. We also include MMB and MMB-CN (Liu et al. 2024c) to study the multilingual ability of VLM since some approaches rely on the CLIP text encoder to work and draw back on non-English tasks.

Comparisons. We compare HiPrune with 7 SOTA visual token reduction methods: ToMe (Bolya et al. 2023b), FastV (Chen et al. 2024a), SparseVLM (Zhang et al. 2025e), HiRED (Arif et al. 2025), TRIM (Song et al. 2025), VisionZip (Yang et al. 2025b), and PyramidDrop (Xing et al. 2025). Some comparisons on Qwen are missing because the corresponding method either can only be applied to LLaVA or does not open-source code.

Method	MMB	MMB ^{CN}	POPE	SQA ^{IMG}	VizWiz	Avg
<i>Vanilla, 2880 Tokens (100%)</i>						
LLaVA	65.8	57.3	86.8	67.5	55.2	100%
<i>Retain 640 Tokens (22.2%)</i>						
FastV	63.1	53.5	79.5	67.4	53.9	95.7%
HiRED	66.0	57.0	85.0	68.3	59.1	101.2%
TRIM	66.8	55.8	86.9	66.9	54.8	99.5%
VisionZip	66.3	58.1	86.3	68.1	57.1	101.2%
SpaVLM	65.9	58.6	85.3	67.6	53.6	99.6%
PDrop	64.1	55.2	83.8	66.7	53.8	97.3%
HiPrune	67.0	59.3	85.3	68.0	59.9	102.6%
<i>Retain 320 Tokens (11.1%)</i>						
FastV	53.4	42.5	49.5	66.6	51.3	80.8%
HiRED	64.2	56.4	83.3	66.8	58.3	99.3%
TRIM	63.5	51.0	86.5	66.2	53.5	96.0%
VisionZip	63.1	55.6	82.1	67.3	56.2	97.8%
SpaVLM	63.1	56.7	76.9	67.2	54.2	96.2%
PDrop	55.5	44.7	60.8	66.7	49.7	84.3%
HiPrune	65.3	57.0	78.9	67.3	59.9	99.5%
<i>Retain 160 Tokens (5.6%)</i>						
TRIM	61.6	45.2	84.8	65.5	52.9	92.6%
VisionZip	60.1	50.4	74.8	68.3	55.5	93.5%
HiPrune	59.8	50.7	67.7	68.7	57.2	92.5%

Table 3: **Results on LLaVA-NeXT-7B.** ‘SpaVLM’ and ‘PDrop’ are abbreviations of SparseVLM (Zhang et al. 2025e) and PyramidDrop (Xing et al. 2025), respectively. Comparison results are reported from (Zhang et al. 2025c).

Implementation Details. We follow the default settings for each compared method as specified in their code repositories. In HiPrune, for both LLaVA-1.5-7B and LLaVA-Next-7B, we set $l = 9$ and $\alpha = 0.1$. For Qwen, we set $l = 16$ and $\alpha = 0.1$ since it has more layers in the vision encoder. Most of the evaluations are performed with the LMMs-Eval toolkit (Zhang et al. 2024), and FLOPs are computed with the calfflops package. All the experiments are conducted on one NVIDIA A100-PCIE (40G).

Main Results

Results on LLaVA-1.5. We first deploy HiPrune on LLaVA-1.5-7B and present comparison results in Table 2 with 192, 128, and 64 tokens retained as the common practice. Across all the settings, HiPrune consistently outperforms existing methods, demonstrating superior performance. Specifically, with **1/3** tokens retained, HiPrune preserves **99.3%** of the original model’s average performance, almost matching the vanilla model. Even under more constrained budgets, HiPrune maintains robust results, achieving **97.5%** with **128** tokens and **92.7%** with just **64** tokens.

Results on LLaVA-NeXT. In Table 3 we present evaluations on LLaVA-NeXT-7B (Liu et al. 2024b), a high-resolution VLM with more visual tokens. When retaining only **22.2%** visual tokens, HiPrune performs even better than the base model, gaining a slight improvement of

Method	MMB	MMB ^{CN}	POPE	SQA ^{IMG}	VizWiz	Avg
<i>Vanilla, 100% Tokens</i>						
Qwen	77.3	73.0	87.0	80.4	68.3	100 %
<i>Retain 33.3% Tokens</i>						
FastV	74.4	70.6	85.0	79.3	66.9	97.4%
VisionZip	74.9	69.8	85.4	80.1	67.1	97.7%
HiPrune	75.8	71.3	86.0	80.0	67.5	98.6%
<i>Retain 22.2% Tokens</i>						
FastV	72.4	69.2	82.7	79.6	66.2	95.9%
VisionZip	73.5	67.4	84.6	80.0	66.3	96.2%
HiPrune	74.0	69.3	84.7	80.3	66.5	97.1%
<i>Retain 11.1% Tokens</i>						
FastV	56.2	60.7	73.3	79.3	63.8	86.4%
VisionZip	67.8	63.3	80.2	79.5	62.8	91.5%
HiPrune	69.6	65.2	80.4	78.9	64.2	92.8%

Table 4: **Results on Qwen2.5-VL-3B-Instruct.** All the results are reproduced by us.

Setting	GQA	MME	POPE	VizWiz	Avg
<i>(a) Attention Pattern</i>					
CLS Token	59.4	1772	85.4	55.5	99.8%
Global*	59.2	1814	86.1	54.5	100.0%
<i>(b) Token Type</i>					
w/o Register	58.4	1693	85.5	54.7	97.9%
w/o Buffer	59.1	1807	85.9	54.2	99.7%
w/o Buf+Anc	59.1	1805	85.9	54.4	99.7%
Full*	59.2	1814	86.1	54.5	100.0%
<i>(c) Selection Scheme</i>					
Square(8)	59.2	1817	86.0	54.4	100.0%
Row(2)	59.2	1795	85.9	54.3	99.6%
Cross(4)*	59.2	1814	86.1	54.5	100.0%

Table 5: **Ablation Study.** Each set is evaluated on LLaVA-1.5-7B with 192 tokens and $\alpha = 0.1$. The number in row (c) denotes buffer token number. ‘*’ denotes the default setting.

2.6%. When only **11.1%** and **5.6%** of tokens are retained, HiPrune still preserves **99.5%** and **92.5%** performance, respectively, demonstrating robustness under extreme circumstances where the token budget is constrained.

Results on Qwen. To verify the versatility of HiPrune, we further insert it into Qwen2.5-VL (Bai et al. 2025) in Table 4. Unlike CLIP, some approaches relying on the text encoder or special tokens may have limited performance or cannot be implemented. When applied to Qwen, HiPrune achieves SOTA performance across the three settings. At an **11.1%** retention rate, HiPrune preserves **92.8%** of the model’s original performance, outperforming FastV and VisionZip by **6.4%** and **1.3%**, respectively. The results on the Qwen series further support our key insights on vision encoders, regardless of their pre-training data or architecture.

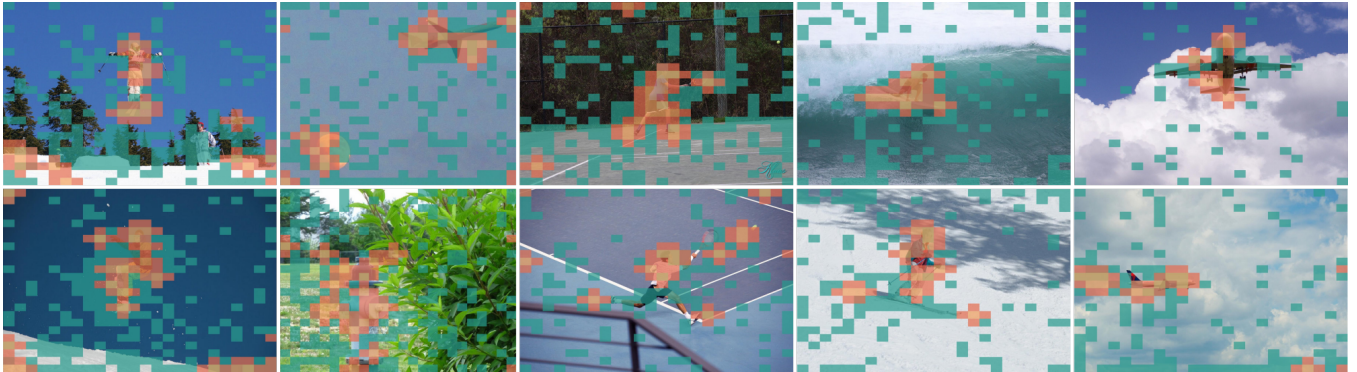


Figure 6: **Visualization on tokens retained by HiPrune.** Anchor tokens are in yellow, buffer tokens are in red, and register tokens are in cyan. Anchor and buffer tokens focus on the sports player, the aircraft, and the fire extinguisher. We set $\alpha = 0.5$ for a better visualization. The images are slightly resized, randomly chosen from the COCO val2017 set (Lin et al. 2014).

Ablation Studies

Attention Pattern. Many methods prune tokens guided by the `CLS` token’s attention to other tokens; however, not every model has this token, making these methods model-specific. We compare computing attention score $\mathbf{a}^{[l]}$ by Eq. 3 and `CLS` in Table 5(a). For our method, the global attention achieves slightly better results and features much stronger versatility since it is model-agnostic.

Token Types. We examine the retained anchor, buffer, and register tokens in HiPrune. As Table 5(b) shows, removing either type degrades the model’s performance. Specifically, removing register tokens causes significant degradation, suggesting the critical role of global information.

Selection Scheme. In Table 5(c) we present different buffer token selection schemes. A square or cross can both achieve similar results; however, when the size of the buffer is too small or missing (row 2 in (b)), the results begin to drop. The buffer tokens are introduced to resist the noise in the attention map, when the window is too small, the effects of the buffer become limited, causing this performance drop.

Object Layer Setting. We conduct a series of benchmarks with different object layer l in Fig. 7. The results indicate that when anchor and buffer tokens are selected from layers 5-9, the overall performance achieves an optimal. It is worth noting that, as Fig. 4 shows, these layers are exactly where high-attention tokens get closest and concentrate on objects, meeting the requirements of object-guidance.

Visualizations and Analyses

Selected Tokens. In Fig. 6 we present a visualization of retained tokens. Anchor tokens and buffer tokens are mainly distributed on the main objects of the image, such as the body of the player, the aircraft in the sky, etc. Preserving these tokens can bring more information about image details and alleviate hallucination. The register tokens diffuse among the whole image uniformly. Despite showing little correlation with image segmentation, they carry indispensable global information. The reason has been discussed in

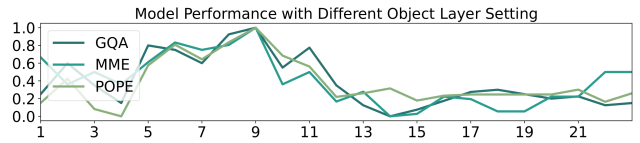


Figure 7: **HiPrune performance on LLaVA-1.5-7B with different l .** The data is normalized for a better comparison.

Token Num	FLOPs (T)↓	Prefill (ms)↓	Decode (ms)↓	VRAM (GB)↓	Throughput (tokens/s)↑
2880	40.57	272.0	26.4	16.5	40.8
640	10.97	62.8	23.9	14.6	41.2
320	6.74	36.3	23.9	14.6	41.3
160	4.63	29.7	23.4	14.6	42.4

Table 6: **Efficiency analyses.** We evaluate HiPrune on LLaVA-NeXT-7B in `bfloat16` and `eager` attention implementation on one A100-PCIE (40G).

our Motivated Insights. The combination of these tokens strikes a balance between overall and detail information.

Efficiency Analyses. We conduct a study of HiPrune inference efficiency on LLaVA-NeXT. We randomly select a sample from the POPE dataset and conduct the experiment 10 times to get an average. As shown in Table 6, with **320** tokens retained, HiPrune preserves **99.5%** of performance with **1.6%** of FLOPs. When the token number is reduced to **160**, the total FLOPs and prefill time are reduced by **8.8×** and **9.2×**, along with less decode latency and GPU memory usage, while sacrificing only **7.5%** performance.

Conclusion

In this paper, we investigate the layer-wise attention patterns of vision encoders and reveal that middle layers predominantly capture object-centric features, while deeper layers emphasize global representations. Motivated by this insight, we propose HiPrune, a model-agnostic and training-free to-

ken pruning method for VLMs that leverages the hierarchical attention structure within the vision encoder. HiPrune strategically selects anchor, buffer, and register tokens to effectively balance computational efficiency and model performance. Extensive experiments across diverse VLM architectures demonstrate the robustness and generality of HiPrune, which consistently achieves state-of-the-art results while significantly reducing computational overhead. We believe our findings offer valuable perspectives on the internal representation of vision encoders and anticipate that HiPrune will facilitate more efficient deployment of VLMs and inspire future research in this direction.

References

Alvar, S. R.; Singh, G.; Akbari, M.; and Zhang, Y. 2025. Diverprune: Diversity-based visual token pruning for large multimodal models. In *CVPR*, 9392–9401.

Arif, K. H. I.; Yoon, J.; Nikolopoulos, D. S.; Vandieren-donck, H.; John, D.; and Ji, B. 2025. HiRED: Attention-Guided Token Dropping for Efficient Inference of High-Resolution Vision-Language Models. In *AAAI*, 1773–1781.

Assran, M.; Bardes, A.; Fan, D.; Garrido, Q.; Howes, R.; Muckley, M.; Rizvi, A.; Roberts, C.; Sinha, K.; Zholus, A.; et al. 2025. V-jepa 2: Self-supervised video models enable understanding, prediction and planning. *arXiv preprint arXiv:2506.09985*.

Bai, J.; Bai, S.; Yang, S.; Wang, S.; Tan, S.; Wang, P.; Lin, J.; Zhou, C.; and Zhou, J. 2023. Qwen-vl: A frontier large vision-language model with versatile abilities. *arXiv preprint arXiv:2308.12966*, 1(2): 3.

Bai, S.; Chen, K.; Liu, X.; Wang, J.; Ge, W.; Song, S.; Dang, K.; Wang, P.; Wang, S.; Tang, J.; et al. 2025. Qwen2. 5-vl technical report. *arXiv preprint arXiv:2502.13923*.

Bolya, D.; Fu, C.-Y.; Dai, X.; Zhang, P.; Feichtenhofer, C.; and Hoffman, J. 2023a. Token Merging: Your ViT but Faster. In *ICLR*.

Bolya, D.; Fu, C.-Y.; Dai, X.; Zhang, P.; Feichtenhofer, C.; and Hoffman, J. 2023b. Token merging: Your vit but faster. In *ICLR*.

Cen, J.; Yu, C.; Yuan, H.; Jiang, Y.; Huang, S.; Guo, J.; Li, X.; Song, Y.; Luo, H.; Wang, F.; et al. 2025. WorldVLA: Towards Autoregressive Action World Model. *arXiv preprint arXiv:2506.21539*.

Chen, L.; Zhao, H.; Liu, T.; Bai, S.; Lin, J.; Zhou, C.; and Chang, B. 2024a. An image is worth 1/2 tokens after layer 2: Plug-and-play inference acceleration for large vision-language models. In *ECCV*, 19–35. Springer.

Chen, Z.; Wang, W.; Tian, H.; Ye, S.; Gao, Z.; Cui, E.; Tong, W.; Hu, K.; Luo, J.; Ma, Z.; et al. 2024b. How far are we to gpt-4v? closing the gap to commercial multimodal models with open-source suites. In *CVPR*.

Dao, T.; Fu, D.; Ermon, S.; Rudra, A.; and Ré, C. 2022. Flashattention: Fast and memory-efficient exact attention with io-awareness. *NeruIPS*, 16344–16359.

Darcet, T.; Oquab, M.; Mairal, J.; and Bojanowski, P. 2024. Vision transformers need registers. In *ICLR*.

Dosovitskiy, A.; Beyer, L.; Kolesnikov, A.; Weissenborn, D.; Zhai, X.; Unterthiner, T.; Dehghani, M.; Minderer, M.; Heigold, G.; Gelly, S.; et al. 2021. An image is worth 16x16 words: Transformers for image recognition at scale. In *ICLR*.

Fu, C.; Chen, P.; Shen, Y.; Qin, Y.; Zhang, M.; Lin, X.; Yang, J.; Zheng, X.; Li, K.; Sun, X.; Wu, Y.; and Ji, R. 2024. MME: A Comprehensive Evaluation Benchmark for Multi-modal Large Language Models. *arXiv:2306.13394*.

Goyal, Y.; Khot, T.; Summers-Stay, D.; Batra, D.; and Parikh, D. 2017. Making the V in VQA Matter: Elevating the Role of Image Understanding in Visual Question Answering. In *CVPR*.

Guo, Z.; Xu, R.; Yao, Y.; Cui, J.; Ni, Z.; Ge, C.; Chua, T.-S.; Liu, Z.; and Huang, G. 2024. Llava-uhd: an lmm perceiving any aspect ratio and high-resolution images. In *ECCV*, 390–406. Springer.

Gurari, D.; Li, Q.; Stangl, A. J.; Guo, A.; Lin, C.; Grauman, K.; Luo, J.; and Bigham, J. P. 2018. Vizwiz grand challenge: Answering visual questions from blind people. In *CVPR*, 3608–3617.

He, K.; Chen, X.; Xie, S.; Li, Y.; Dollár, P.; and Girshick, R. 2022. Masked autoencoders are scalable vision learners. In *CVPR*, 16000–16009.

Hong, W.; Yu, W.; Gu, X.; Wang, G.; Gan, G.; Tang, H.; Cheng, J.; Qi, J.; Ji, J.; Pan, L.; et al. 2025. GLM-4.1 V-Thinking: Towards Versatile Multimodal Reasoning with Scalable Reinforcement Learning. *arXiv preprint arXiv:2507.01006*.

Hu, W.; Dou, Z.-Y.; Li, L. H.; Kamath, A.; Peng, N.; and Chang, K.-W. 2024. Matryoshka Query Transformer for Large Vision-Language Models. *arXiv:2405.19315*.

Hudson, D. A.; and Manning, C. D. 2019. Gqa: A new dataset for real-world visual reasoning and compositional question answering. In *CVPR*, 6700–6709.

Hurst, A.; Lerer, A.; Goucher, A. P.; Perelman, A.; Ramesh, A.; Clark, A.; Ostrow, A.; Welihinda, A.; Hayes, A.; Radford, A.; et al. 2024. Gpt-4o system card. *arXiv preprint arXiv:2410.21276*.

Kim, M. J.; Pertsch, K.; Karamcheti, S.; Xiao, T.; Balakrishna, A.; Nair, S.; Rafailov, R.; Foster, E.; Lam, G.; Sanketi, P.; et al. 2024. Openvla: An open-source vision-language-action model. In *CoRL*.

Li, J.; Li, D.; Savarese, S.; and Hoi, S. 2023a. Blip-2: Bootstrapping language-image pre-training with frozen image encoders and large language models. In *ICML*, 19730–19742. PMLR.

Li, Y.; Du, Y.; Zhou, K.; Wang, J.; Zhao, W. X.; and Wen, J.-R. 2023b. Evaluating object hallucination in large vision-language models. *arXiv preprint arXiv:2305.10355*.

Liang, Z.; Xu, Y.; Hong, Y.; Shang, P.; Wang, Q.; Fu, Q.; and Liu, K. 2024. A Survey of Multimodel Large Language Models. In *Proceedings of the 3rd International Conference on Computer, Artificial Intelligence and Control Engineering*, 405–409.

Lin, T.-Y.; Maire, M.; Belongie, S.; Hays, J.; Perona, P.; Ramanan, D.; Dollár, P.; and Zitnick, C. L. 2014. Microsoft coco: Common objects in context. In *ECCV*, 740–755. Springer.

Liu, H.; Li, C.; Li, Y.; and Lee, Y. J. 2024a. Improved baselines with visual instruction tuning. In *CVPR*, 26296–26306.

Liu, H.; Li, C.; Li, Y.; Li, B.; Zhang, Y.; Shen, S.; and Lee, Y. J. 2024b. LLaVA-NeXT: Improved reasoning, OCR, and world knowledge.

Liu, H.; Li, C.; Wu, Q.; and Lee, Y. J. 2023. Visual instruction tuning. In *NeurIPS*, 34892–34916.

Liu, Y.; Duan, H.; Zhang, Y.; Li, B.; Zhang, S.; Zhao, W.; Yuan, Y.; Wang, J.; He, C.; Liu, Z.; et al. 2024c. Mmbench: Is your multi-modal model an all-around player? In *ECCV*, 216–233. Springer.

Lu, P.; Mishra, S.; Xia, T.; Qiu, L.; Chang, K.-W.; Zhu, S.-C.; Tafjord, O.; Clark, P.; and Kalyan, A. 2022. Learn to Explain: Multimodal Reasoning via Thought Chains for Science Question Answering. In *NeurIPS*.

Maaten, L. v. d.; and Hinton, G. 2008. Visualizing data using t-SNE. *Journal of machine learning research*, 9(Nov): 2579–2605.

Paszke, A.; Gross, S.; Massa, F.; Lerer, A.; Bradbury, J.; Chanan, G.; Killeen, T.; Lin, Z.; Gimelshein, N.; Antiga, L.; et al. 2019. Pytorch: An imperative style, high-performance deep learning library. *NeurIPS*, 32.

Radford, A.; Kim, J. W.; Hallacy, C.; Ramesh, A.; Goh, G.; Agarwal, S.; Sastry, G.; Askell, A.; Mishkin, P.; Clark, J.; et al. 2021. Learning transferable visual models from natural language supervision. In *ICML*, 8748–8763. PMLR.

Singh, A.; Natarajan, V.; Shah, M.; Jiang, Y.; Chen, X.; Batra, D.; Parikh, D.; and Rohrbach, M. 2019. Towards vqa models that can read. In *CVPR*, 8317–8326.

Song, D.; Wang, W.; Chen, S.; Wang, X.; Guan, M.; and Wang, B. 2025. Less is more: A simple yet effective token reduction method for efficient multi-modal llms. In *COLING*.

Team, G.; Anil, R.; Borgeaud, S.; Alayrac, J.-B.; Yu, J.; Soricut, R.; Schalkwyk, J.; Dai, A. M.; Hauth, A.; Millican, K.; et al. 2023. Gemini: a family of highly capable multimodal models. *arXiv preprint arXiv:2312.11805*.

Touvron, H.; Cord, M.; Douze, M.; Massa, F.; Sablayrolles, A.; and Jégou, H. 2021. Training data-efficient image transformers & distillation through attention. In *ICML*, 10347–10357. PMLR.

Touvron, H.; Lavril, T.; Izacard, G.; Martinet, X.; Lachaux, M.-A.; Lacroix, T.; Rozière, B.; Goyal, N.; Hambro, E.; Azhar, F.; et al. 2023. Llama: Open and efficient foundation language models. *arXiv preprint arXiv:2302.13971*.

Vaswani, A.; Shazeer, N.; Parmar, N.; Uszkoreit, J.; Jones, L.; Gomez, A. N.; Kaiser, Ł.; and Polosukhin, I. 2017. Attention is all you need. In *NeurIPS*.

Xing, L.; Huang, Q.; Dong, X.; Lu, J.; Zhang, P.; Zang, Y.; Cao, Y.; He, C.; Wang, J.; Wu, F.; et al. 2025. Pyramiddrop: Accelerating your large vision-language models via pyramid visual redundancy reduction. In *CVPR*.

Yang, A.; Li, A.; Yang, B.; Zhang, B.; Hui, B.; Zheng, B.; Yu, B.; Gao, C.; Huang, C.; Lv, C.; et al. 2025a. Qwen3 technical report. *arXiv preprint arXiv:2505.09388*.

Yang, J.; Luo, K. Z.; Li, J.; Deng, C.; Guibas, L.; Krishnan, D.; Weinberger, K. Q.; Tian, Y.; and Wang, Y. 2024. Denoising vision transformers. In *ECCV*, 453–469. Springer.

Yang, S.; Chen, Y.; Tian, Z.; Wang, C.; Li, J.; Yu, B.; and Jia, J. 2025b. Visionzip: Longer is better but not necessary in vision language models. In *CVPR*, 19792–19802.

Zhai, X.; Mustafa, B.; Kolesnikov, A.; and Beyer, L. 2023. Sigmoid loss for language image pre-training. In *ICCV*, 11975–11986.

Zhang, K.; Li, B.; Zhang, P.; Pu, F.; Cahyono, J. A.; Hu, K.; Liu, S.; Zhang, Y.; Yang, J.; Li, C.; and Liu, Z. 2024. LMMs-Eval: Reality Check on the Evaluation of Large Multimodal Models. *arXiv:2407.12772*.

Zhang, Q.; Cheng, A.; Lu, M.; Zhang, R.; Zhuo, Z.; Cao, J.; Guo, S.; She, Q.; and Zhang, S. 2025a. Beyond Text-Visual Attention: Exploiting Visual Cues for Effective Token Pruning in VLMs. In *ICCV*.

Zhang, Q.; Cheng, A.; Lu, M.; Zhuo, Z.; Wang, M.; Cao, J.; Guo, S.; She, Q.; and Zhang, S. 2025b. [CLS] Attention is All You Need for Training-Free Visual Token Pruning: Make VLM Inference Faster. In *ICCV*.

Zhang, Q.; Liu, M.; Li, L.; Lu, M.; Zhang, Y.; Pan, J.; She, Q.; and Zhang, S. 2025c. Beyond Attention or Similarity: Maximizing Conditional Diversity for Token Pruning in MLLMs. *arXiv preprint arXiv:2506.10967*.

Zhang, S.; Fang, Q.; Yang, Z.; and Feng, Y. 2025d. LLaVA-Mini: Efficient Image and Video Large Multimodal Models with One Vision Token. In *ICLR*.

Zhang, Y.; Fan, C.-K.; Ma, J.; Zheng, W.; Huang, T.; Cheng, K.; Gudovskiy, D.; Okuno, T.; Nakata, Y.; Keutzer, K.; et al. 2025e. SparseVLM: Visual Token Sparsification for Efficient Vision-Language Model Inference. In *ICML*.

Pseudo-code for HiPrune

In Algorithm 1, we provide a pseudo-code for HiPrune written in PyTorch style (Paszke et al. 2019) to better explain our method. This example is adapted from LLaVA and adopts the `cross` as the strategy to select buffer tokens.

Algorithm 1: HiPrune with `cross` selection scheme.

Input: Image tensor `image`
Parameter: Token Budget `N`, Object Layer 1, Object Proportion `alpha`, Encoder Patch Size `p`
Output: Pruned token tensor `retained_tokens`

```

1 tokens, all_attns = encoder(image)
2 ## Compute attention score from object layer 1
3 mid_attn = all_attns[1].squeeze(0) # Remove batch
4 mid_attn = mid_attn.mean(0) # Average multi-head
5 mid_attn = mid_attn.sum(0) # Attention to each token
6 mid_attn = mid_attn[1:] # Exclude cls
7 ## Assign anchor tokens
8 a_sum = round(N * alpha / 5) # 5 tokens in a cluster
9 a_idx = topk(mid_attn, k=a_sum).indices
10 ## Assign buffer tokens
11 b_idx = cat([a_idx-1, a_idx+1, a_idx-p, a_idx+p])
12 a_b_idx = unique(cat([a_idx, b_idx]).clamp(0, p**2))
13 ## Compute attention score from output layer
14 deep_attn = all_attns[-1].squeeze(0)
15 deep_attn = mid_attn.mean(0).sum(0)[1:]
16 ## Assign register tokens
17 mask = zeros(N).scatter_(a_b_idx, 1)
18 deep_attn = deep_attn - mask # Mask already-chosens
19 r_sum = N - a_b_idx.shape[0]
20 r_idx = topk(deep_attn, k=r_sum).indices
21 ## Retain these tokens
22 retained_idx = cat([a_idx, b_idx, r_idx])
23 retained_tokens = tokens[retained_idx]
24 return retained_tokens

```

Hierarchical Attention Pattern Details

In Fig. 2, we show how attention distribution shifts across layers in CLIP. Here, we explain details about Fig. 2(a) and Fig. 2(b). Since HiPrune prunes visual tokens by their rankings rather than absolute values, we focus on the ranking of each token’s attention. In Alg. 2, we state our acquisition process of Fig. 2(a), which shows the ranking of attentions across layers. In Fig. 2(b), it is worth noting that each dot (regardless of color) is the projected token **from the output layer**, and the color does not mean that the token is drawn from middle layers. We have included a comprehensive visualization in the next section.

Visualization of Attention Evolution

As shown in Fig. 9, the high-attention tokens in the input layer and the output layer (last but one in LLaVA) obey distinct distributions. In these examples, high-attention tokens in the shallow layer distribute uniformly across the embedding space, while they cluster in the output layer. During the shift, the middle layers show a transitional status covering every cluster. These examples indicate that CLIP encodes images in a continuous and gradual way, forming a hierarchical representation inside the vision encoder.

Algorithm 2: Acquisition process of Fig. 2(a).

Input: Image tensor `image`

Output: Attention Ranking Coordinates `coor_2d`

```

1 all_ranks = []
2 tokens, all_attns = encoder(image)
3 for attn in all_attns:
4     ## Same attn extraction process in Alg. 1
5     attn = attn.squeeze(0)
6     attn = attn.mean(0).sum(0)[1:]
7     ## Transform attn values into ranks
8     ## [0.2, 0.3, 0.5, 0.1] -> [1, 2, 3, 0]
9     attn_rank = argsort(argsort(attn)) # [1, 576]
10    all_ranks.append(attn_rank)
11 all_ranks = stack(all_ranks, dim=0) # [24, 576]
12 tsne = TSNE(n_components=2) # Project into 2D space
13 coor_2d = tsne.fit_transform(all_ranks) # [24, 2]
14 return coor_2d # plt.scatter(coor_2d)

```

Model Name	Huggingface Model Path
CLIP-L / CLIP	openai/clip-vit-large-patch14-336
CLIP-B	openai/clip-vit-base-patch32
SigLIP	google/siglip-so400m-patch14-384
SigLIP2	google/siglip2-so400m-patch14-384
DeiT	facebook/deit-base-patch16-224
VJEP2	facebook/vjepa2-vitl-fpc64-256
LLaVA-1.5-7B	liuhaojian/llava-v1.5-7b
LLaVA-1.5-13B	liuhaojian/llava-v1.5-13b
LLaVA-NeXT-7B	liuhaojian/llava-v1.6-vicuna-7b
Qwen2.5-VL-3B-Instruct	Qwen/Qwen2.5-VL-3B-Instruct
Qwen2.5-VL-7B-Instruct	Qwen/Qwen2.5-VL-7B-Instruct

Table 7: Mapping table between the model name in this paper and the corresponding Huggingface path.

Evaluation Details

For HiPrune, most of our evaluations are completed with LMMs-Eval toolkit (Zhang et al. 2024). However, since some benchmarks either are extremely slow on LMMs-Eval or need Internet for an online evaluation, the MMB, MMB-CN (Liu et al. 2024c), TextVQA (Singh et al. 2019), and VQAv2 (Goyal et al. 2017) results in Table 2 are obtained with the public codebase released by LLaVA (Liu et al. 2023). The rest of the results in Table 2 and all the results in Tables 3 and 4 are obtained with LMMs-Eval.

Model Details

All the models utilized in this paper are downloaded from Huggingface. Here, we provide the mapping table between the notes and online model path in Table 7.

Extended Experiment Results

We further apply HiPrune to LLaVA-1.5-13B, LLaVA-NeXT-13B, and Qwen2.5-VL-7B-Instruct (Liu et al. 2023, 2024a; Bai et al. 2025). These experiments follow the same experiment settings described in Section Experiment. The results for LLaVA-series are reported in Table 8, and the results for Qwen-series are in Table 9. When implemented on a model with a different size, HiPrune maintains its overall performance and shows a trend similar to a smaller one reported in our paper. Notably, for SQA and VizWiz, HiPrune acquires results even slightly better than baseline

Method	Token Num	GQA	MMB	MMB ^{CN}	MME	POPE	SQA ^{IMG}	VQA ^{V2}	VQA ^{Text}	VizWiz
LLaVA-1.5-13B	576	63.2	67.7	63.5	1818	85.9	72.8	80.0	61.3	53.6
	192	59.4	67.1	62.5	1798	85.4	73.7	78.0	59.5	55.6
	128	57.9	66.8	63.1	1730	82.8	74.1	76.1	58.3	54.9
	64	54.2	64.8	59.2	1634	72.4	74.6	70.3	56.7	56.0
LLaVA-NeXT-13B	2880	64.4	68.5	61.2	1901	85.3	73.1	82.3	63.2	59.1
	640	62.6	70.2	65.3	1877	84.9	71.6	80.0	61.6	61.1
	320	59.3	68.6	64.9	1800	79.7	72.1	75.7	60.1	59.2
	160	54.4	66.3	61.3	1647	71.0	70.9	68.4	57.1	55.9

Table 8: Performance comparisons on LLaVA-1.5-13B and LLaVA-NeXT-13B (Liu et al. 2024a).

Method	Token Budget	GQA	MMB	MMB ^{CN}	MME	POPE	SQA ^{IMG}	VQA ^{text}	VizWiz
Qwen2.5-VL-7B	100%	60.5	83.2	80.1	2331	86.2	87.4	83.1	70.4
	33.3%	58.9	82.6	79.5	2303	85.1	86.8	78.2	69.2
	22.2%	57.1	80.3	77.6	2189	84.0	85.3	74.0	68.9
	11.1%	52.5	76.1	73.7	2000	79.8	82.7	62.4	66.9

Table 9: Performance comparisons on Qwen2.5-VL-7B-Instruct (Bai et al. 2025).

under some settings. HiPrune is model-agnostic and easy to deploy on other VLMs, which is among our future works.

Visualizations on Retained Tokens

We provide extended examples on retained tokens in Fig. 8. We can see that the anchor tokens and buffer tokens contain the main body of the image, e.g., the player, the person, and the animal, which are crucial for image understanding. The register tokens seem less image-aligned, but cover the whole image sufficiently, indicating they encode global information. The reason is discussed in the section Experiment, and this visualization further confirms our theory.

Visualizations on All Layers' Attention

We provide two examples of all layers' attention distribution in Fig. 10 and 11. We can see that in the middle layers, the highlighted areas mainly overlap the person, which is the main object of the image, and agrees with the human perception order, as we also first notice the person in the image.

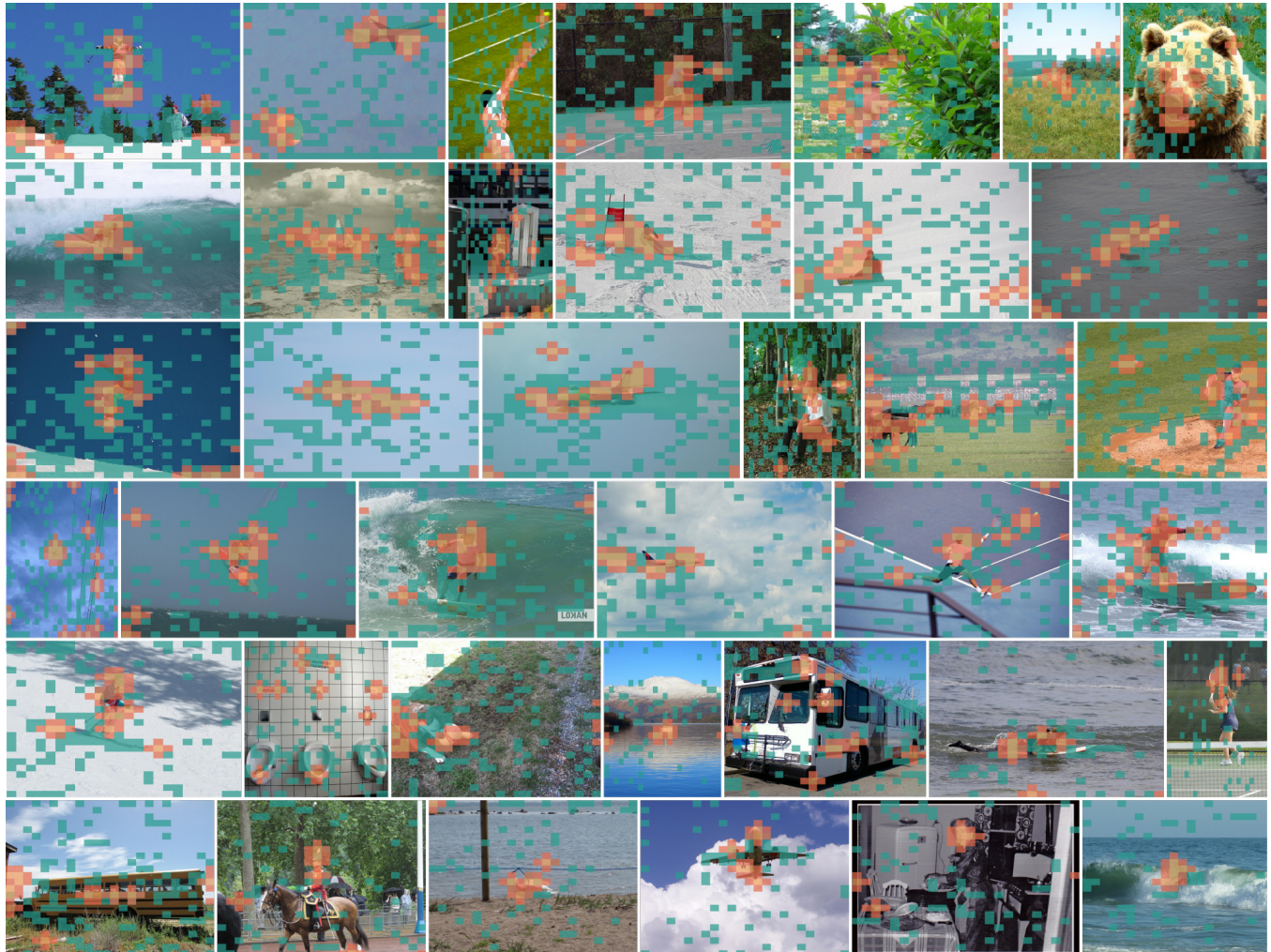


Figure 8: Visualization on tokens retained by HiPrune. The images are randomly chosen from the COCO val2017 set (Lin et al. 2014). Anchor tokens are in yellow, buffer tokens are in red, and register tokens are in cyan.

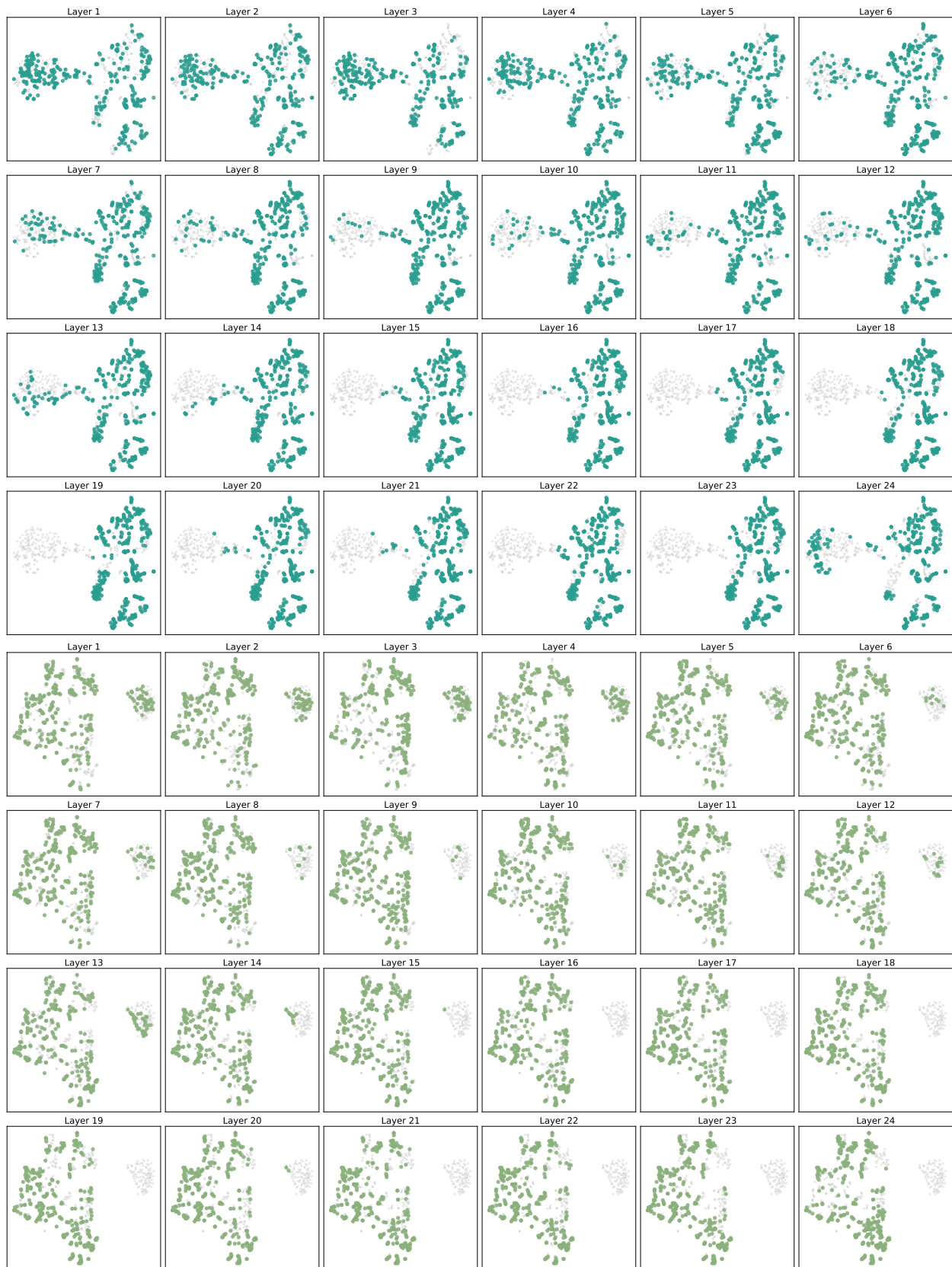


Figure 9: Two examples of t-SNE visualization on visual tokens that receive top 50% attention from different CLIP layers.

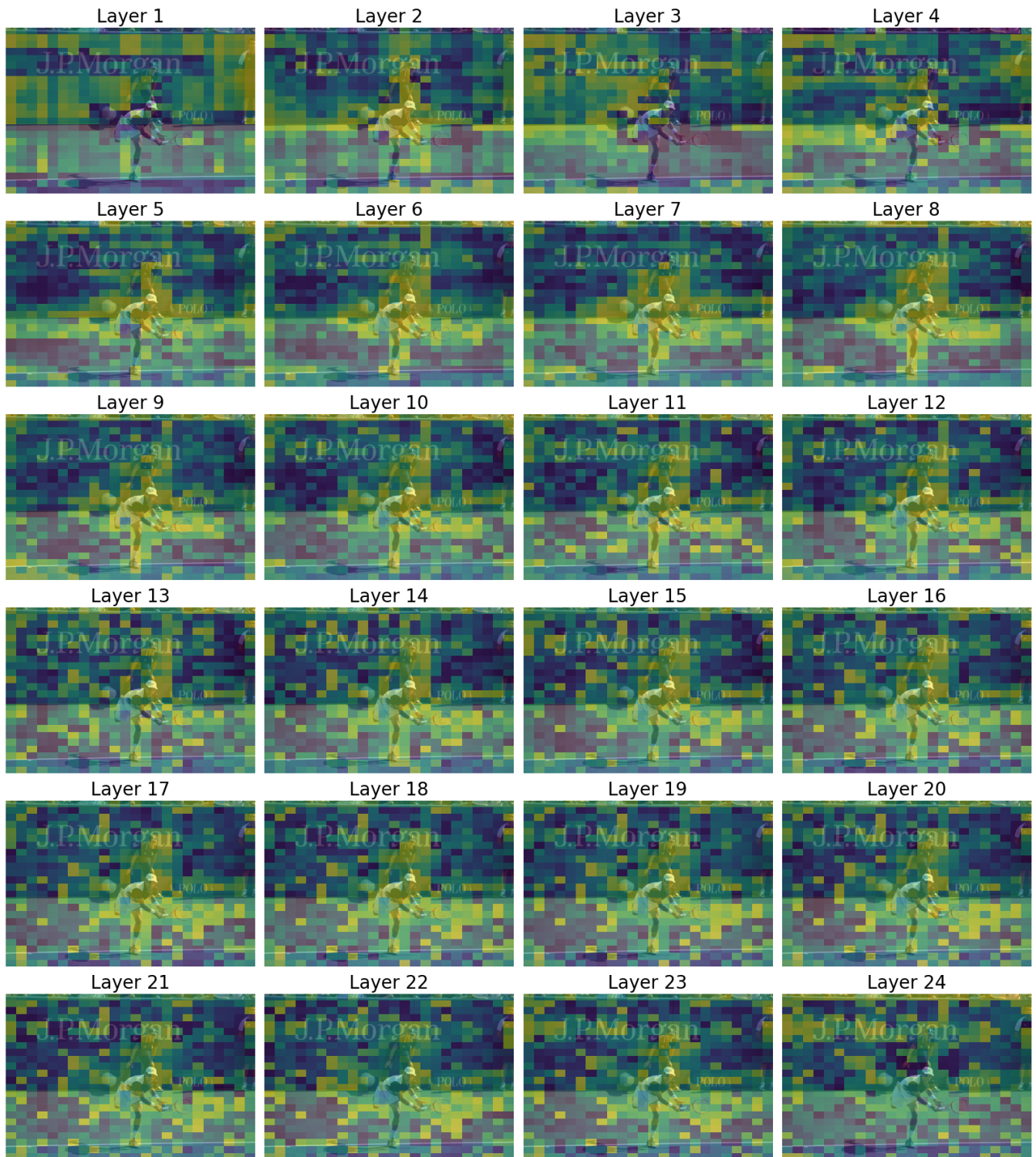


Figure 10: Visualization of all layers' attention in the CLIP model.

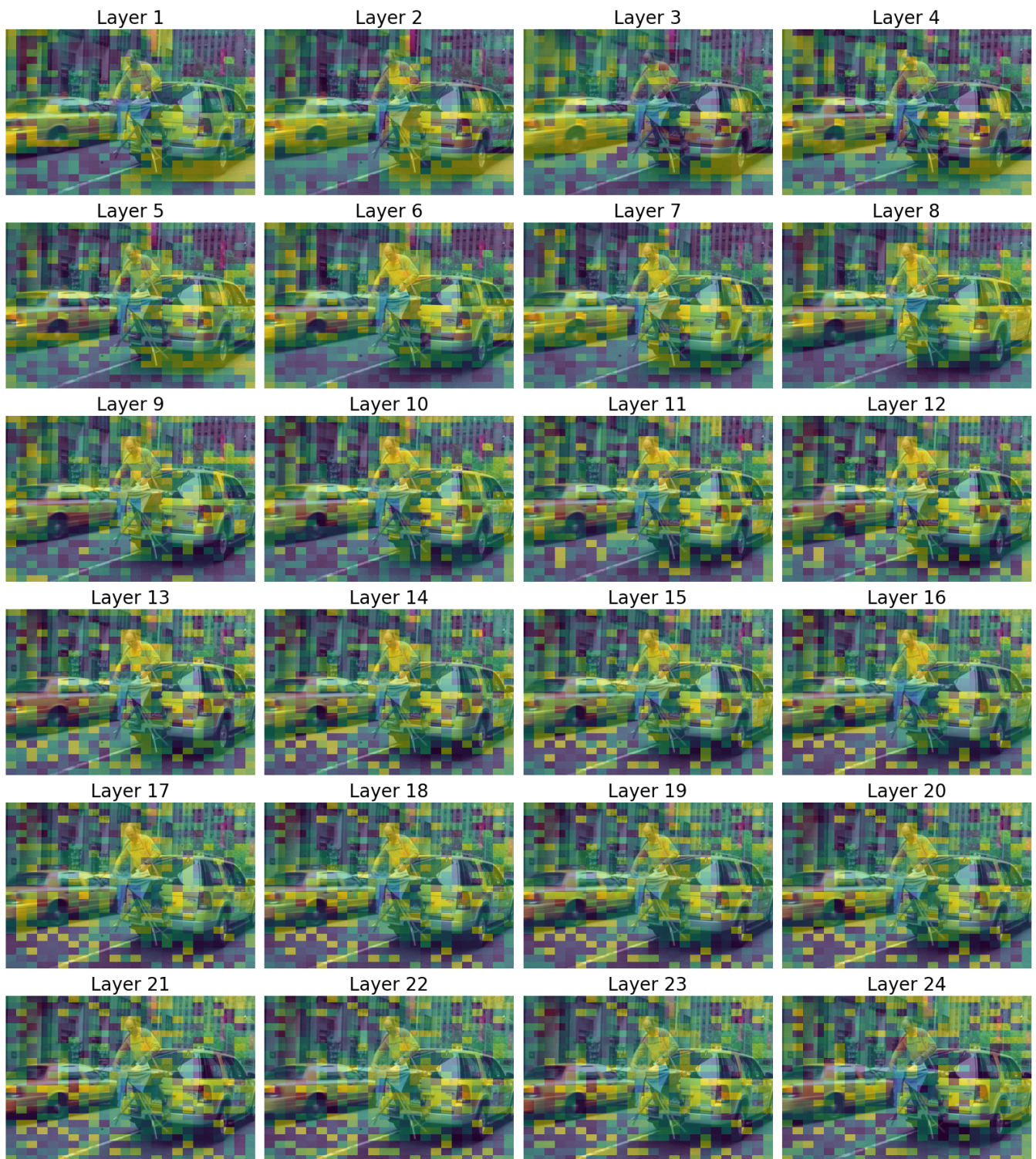


Figure 11: Visualization of all layers' attention in the CLIP model.